JCI insight

Spatial detection and consequences of nonrenal calcitriol production as assessed by targeted mass spectrometry imaging

Mark B. Meyer, … , Diego F. Cobice, J. Wesley Pike

JCI Insight. 2024. https://doi.org/10.1172/jci.insight.181763.

Research In-Press Preview Endocrinology

The immune benefits of vitamin D_3 supplementation beyond calcium and phosphate maintenance are highly clinically debated. Kidney expression of CYP27B1 is the source of endocrine, circulating $1,25(OH)_2D_3$ (active form of vitamin D) that maintains serum calcium and phosphate. $1,25(OH)_2D_3$ may also be made by the CYP27B1 enzyme in non-renal cells, like immune cells, in a process driven by cellular availability of $25(OH)D_3$ and inflammation. Due to the endocrine nature of $1,25(OH)_2D_3$ in circulation, it is difficult to discern between these two sources. We recently created a regulatory deletion model of *Cyp27b1* (M1/M21-DIKO) where mice have normal inflammatory-regulated *Cyp27b1* expression in non-renal tissues (unlike global *Cyp27b1*-KO), but no expression within kidney. Here, utilizing on-tissue chemical derivatization and Matrix Assisted Laser Desorption Ionization-Mass Spectrometry Imaging (MALDI-MSI), we investigated the distribution of $1,25(OH)_2D_3$ and $25(OH)D_3$ in the kidney, liver, spleen, and thymus. MALDI-MSI demonstrated increased $1,25(OH)_2D_3$ in non-renal tissues such as the spleen after vitamin D_3 supplementation in M1/M21-DIKO mice. Additionally, from this we found increased *Il4* and decreased *Tnfa* in the spleen after vitamin D_3 supplementation. Taken together, these data demonstrate non-renal production of $1,25(OH)_2D_3$ in vivo and provide a consequence of vitamin D_3 supplementation and non-renal $1,25(OH)_2D_3$ production in cytokine changes.

Spatial detection and consequences of nonrenal calcitriol production as assessed by targeted mass spectrometry imaging

Mark B. Meyer[1*], Seong Min Lee[1], Shannon R. Cichanski[1], Diego F. Cobice[2], J. Wesley Pike[3]

[1]Department of Nutritional Sciences, University of Wisconsin-Madison, Madison, WI 53706, U.S.A; [2]Mass Spectrometry Centre, Biomedical Sciences Research Institute (BMSRI), School of Biomedical Sciences, Ulster University, Coleraine, Northern Ireland, UK; [3]Department of Biochemistry, University of Wisconsin-Madison, Madison, WI 53706, U.S.A

Running Title: Non-renal calcitriol MSI

*****_To whom correspondence should be addressed: Mark B. Meyer, PhD, Department of Nutritional Sciences, University of Wisconsin-Madison, 1415 Linden Drive, Madison, WI 53706. Phone: (608) 890-8057. Email: markmeyer@wisc.edu_

Keywords: mass spectrometry imaging, vitamin D, 25(OH)D_3, Cytochrome P450, 1,25(OH)$_2D_3$, *Cyp27b1*, *Cyp24a1*

Conflict of interest: The authors declare no conflicts of interest with the contents of this article.

Abstract

The immune benefits of vitamin D_3 supplementation beyond calcium and phosphate maintenance are highly clinically debated. Kidney expression of CYP27B1 is the source of endocrine, circulating $1,25(OH)_2D_3$ (active form of vitamin D) that maintains serum calcium and phosphate. $1,25(OH)_2D_3$ may also be made by the CYP27B1 enzyme in non-renal cells, like immune cells, in a process driven by cellular availability of $25(OH)D_3$ and inflammation. Due to the endocrine nature of $1,25(OH)_2D_3$ in circulation, it is difficult to discern between these two sources. We recently created a regulatory deletion model of *Cyp27b1* (M1/M21-DIKO) where mice have normal inflammatory-regulated *Cyp27b1* expression in non-renal tissues (unlike global *Cyp27b1*-KO), but no expression within kidney. Here, utilizing on-tissue chemical derivatization and Matrix Assisted Laser Desorption Ionization-Mass Spectrometry Imaging (MALDI-MSI), we investigated the distribution of $1,25(OH)_2D_3$ and $25(OH)D_3$ in the kidney, liver, spleen, and thymus. MALDI-MSI demonstrated increased $1,25(OH)_2D_3$ in non-renal tissues such as the spleen after vitamin D_3 supplementation in M1/M21-DIKO mice. Additionally, from this we found increased *Il4* and decreased *Tnfa* in the spleen after vitamin D_3 supplementation. Taken together, these data demonstrate non-renal production of $1,25(OH)_2D_3$ *in vivo* and provide a consequence of vitamin D_3 supplementation and non-renal $1,25(OH)_2D_3$ production in cytokine changes.

Introduction

Vitamin D has profound abilities to regulate many different biological processes such as influence the differentiation of skeletal cells, change immune programming, process bile acids, control mineral channels, fight cancer cell proliferation, and promote anti-inflammatory responses (1-4). The amount of vitamin D_3 supplementation needed for these various tasks however has been widely debated as human clinical trials have failed to confirm the effects observed from cell culture and animal studies (5-7). These studies are all complicated by renal production of $1,25(OH)_2D_3$ (calcitriol) (8). The ability of the body to regulate calcium (Ca) and phosphate (P) relies on proper functioning of vitamin D metabolism with CYP27B1 making $1,25(OH)_2D_3$ and CYP24A1 degrading. *CYP27B1* expression in the kidney is a highly regulated, endocrine

hormone-controlled process with parathyroid hormone (PTH) inducing and fibroblast growth factor 23 (FGF23) and $1,25(OH)_2D_3$ suppressing (8). *CYP24A1* expression is reciprocally regulated to *CYP27B1* in that PTH suppresses and FGF23 and $1,25(OH)_2D_3$ induce (9, 10). The balance of these enzymes in the kidney controls vitamin D metabolism in the body.

Outside of kidney, regulation of *CYP27B1* and *CYP24A1* are quite different. *CYP27B1* expression is not controlled by the endocrine hormones PTH, FGF23, or $1,25(OH)_2D_3$ (10). *CYP24A1* retains its ability to be regulated by $1,25(OH)_2D_3$, however, FGF23 and PTH fail to change the expression in non-renal tissues (9). Additionally, the non-renal expression levels of *Cyp27b1* and *Cyp24a1* are 100- to 1000-fold lower than what is observed in the kidney in mice (9, 10). However, these non-renal cells do retain low and measurable expression of *Cyp27b1*. *Cyp27b1* in these tissues is induced by inflammatory signals like lipopolysaccharides (LPS), IL-1β, and others (11). It has also been demonstrated that macrophages can produce $1,25(OH)_2D_3$ during sarcoidosis in humans (12). Substrate availability ($25(OH)D_3$) for CYP27B1 is key to the physiologic regulation of vitamin D metabolism as $25(OH)D_3$ bound to an albumin binding protein (vitamin D binding protein, DBP) is transported through the cell surface receptors megalin and cubulin (13-15). These receptors have high expression in the kidney, so the availability of $25(OH)D_3$ remains high, however, other tissues have far lower expression and thus, for this reason, it is believed they may have lower availability of $25(OH)D_3$ (16). Additionally, a recent article examining $1,25(OH)_2D_3$ levels in anephric patients found that low levels of circulating $1,25(OH)_2D_3$ were present and this was postulated to be coming from non-renal sources driven by substrate availability (17).

We recently solved the renal regulatory mechanism for *Cyp27b1* expression through key upstream enhancers in the proximal convoluted tubule cells (18) in intronic regions of the neighboring *Mettl1* and *Mettl121b* (*Eef1akmt3*) genes (10, 11). We used CRISPR-Cas9 editing to create a mouse (M1/M21-double intronic knockout, M1/M21-DIKO) with a similar phenotype to the global *Cyp27b1*-KO mouse with low serum calcium and phosphate, low FGF23, very high levels of PTH as well as many skeletal and mineral defects (11). The M1/M21-DIKO mouse had minimal expression of the *Cyp27b1* gene in the kidney and was resistant to endocrine hormone control by PTH, FGF23, or $1,25(OH)_2D_3$. This animal also had altered

vitamin D metabolism with low circulating $1,25(OH)_2D_3$ and elevated levels of $25(OH)D_3$ among other metabolite changes (11). Critically, the M1/M21-DIKO mouse retained its basal expression and inflammatory induction of *Cyp27b1* in non-renal tissues including macrophages and T-cells (11). We described this mouse as a kidney-specific, endocrine-deficient *Cyp27b1* pseudo-null mouse since the effects were confined to the kidney (11). We also demonstrated that, like the global *Cyp27b1*-KO mouse, the M1/M21-DIKO mouse could have its skeleton and mineral defects rescued by feeding a diet high in calcium, phosphate, and lactose (2%, 1.25%, 20% lactose) for 12-16 weeks (11). This reduced the $1,25(OH)_2D_3$ circulating levels below the lower limits of detection (LLOD) in the mouse. Therefore, we believe the dietary rescued M1/M21-DIKO mouse represents the ideal model with which to study vitamin D_3 supplementation and the potential to isolate and demonstrate non-renal production of $1,25(OH)_2D_3$.

Routine and clinical measurements of both $25(OH)D_3$ and $1,25(OH)D_3$ in the serum or plasma are typically made with ELISA kits or a radioimmunoassay (RIA) assay (19), however these methods lack detailed analysis of the multitude of vitamin D metabolite derivatives and can often be confounded by them (20, 21). Methods of liquid chromatography followed by tandem mass spectrometry (LC-MS/MS) greatly increases the ability to see these derivatives in the serum or plasma with absolute quantitation (22). However, detection of tissue levels of vitamin D metabolites is not trivial given the high lipid and cholesterol content of tissues. Further, detecting the potential for production of those metabolites in tissues, as we propose here, is also complicated by the circulating $1,25(OH)_2D_3$ production from the kidney. Recently, methods were developed for the targeted acquisition of spatial identification and relative quantitation of vitamin D metabolites through advances in mass spectrometry imaging (23). Serum detection of vitamin D metabolites by LC-MS/MS involves a chemical derivatization (CD) step to improve the ionization efficiency of steroidal compounds (20, 22). By taking this a step further, the derivatization can be accomplished on tissue sections (on-tissue chemical derivatization, OTCD) to enable tissue detection of vitamin D metabolites. Additionally, spatial information within the tissue can be obtained when linked to MALDI followed by Mass Spectrometry (MS) detection (23). Thus far, this OTCD-MALDI-MSI

pipeline of analysis has been completed to identify both $25(OH)D_3$ and $1,25(OH)_2D_3$ in the mouse kidney of wildtype mice in proof-of-principle experiments (23).

In this current study, we combined this latest technology of MSI utilizing OTCD-MALDI-MSI to identify and quantify the tissue level production of $1,25(OH)_2D_3$ and $25(OH)D_3$. With our M1/M21-DIKO mouse, we have eliminated the circulating $1,25(OH)_2D_3$ and focus on the detection of $1,25(OH)_2D_3$ resident in the tissues themselves. Using this unique MSI technique, we demonstrate detection and spatial location of $1,25(OH)_2D_3$ and $25(OH)D_3$ in tissues outside of the kidney. We hypothesize that vitamin D_3 supplementation will increase $25(OH)D_3$ circulation and tissue availability, as well as the production of $1,25(OH)_2D_3$ in tissues outside of the kidney in the M1/M21-DIKO mouse. This, in turn, may prove beneficial for inflammatory disease amelioration and provide the missing link between cell and human studies. In these studies, we have demonstrated non-renal detection and production of $1,25(OH)_2D_3$ *in vivo*, as well as gene expression consequences, in response to vitamin D_3 supplementation.

Results

Mass spectrometry imaging validation of vitamin D metabolites in wildtype and Cyp27b1-KO mice

We used a similar workflow and procedure as previously reported for mass spectrometry interrogation of targeted metabolite imaging and plasma metabolites from tissues (23), which is summarized in Fig. 1. The mice lacking mature, full-length CYP27B1 protein (*Cyp27b1*-KO) are known to have elevated levels of substrate $25(OH)D_3$ compared to their wildtype (WT) littermates (10, 11). We confirmed these elevated plasma levels of $25(OH)D_3$ and that $1,25(OH)_2D_3$ is absent compared to WT mice, in this study. In Supplemental Figure 1A (Fig. S1A), mice (male and female) were examined by LC-MS/MS for both $25(OH)D_3$ and $1,25(OH)_2D_3$ concentrations in the plasma. WT mice had an average plasma $25(OH)D_3$ concentration of 15.4 ± 1.1 ng/mL and a $1,25(OH)_2D_3$ concentration of 23.7 ± 1.9 pg/mL (Fig. S1), consistent with our prior studies (10, 11). The *Cyp27b1*-KO (C27KO) mice had a $25(OH)D_3$ concentration of 77.9 ± 2.8 ng/mL (Fig. S1) and $1,25(OH)_2D_3$ that was found in the linear range but fell below the lower limit of quantitation (<LLOQ), however these values were above the lower limit of detection (LLOD), and

are therefore included and displayed in red. Plasma LLOQ for $25(OH)D_3$ is ≤ 2 ng/mL and $1,25(OH)_2D_3$ ≤ 5 pg/mL. Both the $25(OH)D_3$ and $1,25(OH)_2D_3$ *Cyp27b1*-KO vs. WT were statistically significant with $p < 0.001$ in each case by t-test analysis. Both male and female mice were included in the replicates, no differences were found and therefore the results are reported as mixed. These mice confirm our previously measured plasma $25(OH)D_3$ and $1,25(OH)_2D_3$ concentrations for both the WT and *Cyp27b1*-KO mice (10, 11).

We then investigated tissue MALDI-MSI for both WT and *Cyp27b1*-KO animals. Both WT and *Cyp27b1*-KO animals were fed a chow diet (3.4 IU/g of vitamin D) until 8 w of age. Mice were then perfused with PBS and tissues were collected. Animal body weights, bone mineral density, serum Ca, P, PTH, and FGF23 are reported in Fig. S3. Importantly, the intratissue systemic contribution of blood was not detected in the tissues, indicating the perfusion was complete as detailed in the Methods. MALDI-MSI was performed for kidney, liver, spleen, and thymus, as seen in Fig. 2. Representative MSI images are shown in Fig. 2 panels A-D with $25(OH)D_3$ (top) and $1,25(OH)_2D_3$ (bottom) of each panel. Relative quantification from the raw MSI data for each panel and biological replicate sample are displayed in Fig. 2F and 2G. Representative images from all biological triplicates and the full table of metabolites are shown in Fig. S2 and Fig. S1, respectively. The current resolution of MSI is based on the laser used for tissue ablation, which is near 35 μm in size, thus ablating ~3-5 cells at a time. As can be observed in Fig. 2A (upper), the WT kidney shows small amounts of $25(OH)D_3$ present indicated by the low ion relative intensity or abundance (lower on scale, lighter blue) compared to areas of high ion relative intensity and abundance (higher on scale, orange and bright yellow). The WT kidney $1,25(OH)_2D_3$ (Fig. 2A, lower) shows a high relative intensity of the $1,25(OH)_2D_3$ metabolite. In contrast to the WT metabolite levels of the $25(OH)D_3$, the *Cyp27b1*-KO mouse (C27KO) has high levels of $25(OH)D_3$. As expected, the *Cyp27b1*-KO mouse is incapable of making $1,25(OH)_2D_3$ and therefore the MSI images show very low levels of ion intensity and metabolite detection. From an overlay of a schematic of the mouse kidney anatomy (Fig. 2E), we find that $1,25(OH)_2D_3$ appears in both the cortex and medulla, with the inner medulla having a much higher relative ion intensity than the cortex or outer medulla. Quantification of these data as shown in Fig.

2F measure the 25(OH)D_3 of the WT kidney to be 34.1 ± 3.1 ng/g and the *Cyp27b1*-KO 98.5 ± 6.1 ng/g. 1,25$(OH)_2D_3$ quantification (Fig. 2G) of WT kidney is 66.4 ± 3.4 pg/g and *Cyp27b1*-KO as 3.8 ± 0.4 pg/g, however, the LLOQ for 1,25$(OH)_2D_3$ by MSI (or by LC-MS/MS) are 5 pg/g therefore, while these numbers were calculated, they appear as red in color in the quantification for below LLOQ. These data validate the method against the prior publication for MSI of vitamin D metabolites (23) and are in line with those measured for the plasma values (Table S1) and from our prior work (10, 11).

The liver is the source of 25(OH)D_3 production by the CYP2R1 enzyme and thus, is expected to have the highest tissue levels of 25(OH)D_3 in the mouse. In Fig. 2B, MSI confirms this expectation as the levels of 25(OH)D_3 are high in both the WT and *Cyp27b1*-KO mice. Quantification of these data in Fig. 2F show there is no statistical difference in the levels of 25(OH)D_3 between the WT and *Cyp27b1*-KO mice (202.5 ± 13.9 and 212.7 ± 11.6 ng/g, respectively, Fig. 2F). The levels of 1,25$(OH)_2D_3$ (Fig. 2G) in the liver are low with 2 of the 3 replicates falling below the LLOQ for both WT (4.4 ± 0.7 pg/g) and *Cyp27b1*-KO (4.5 ± 0.7 pg/g, Fig. 2G). Both spleen and thymus contain very little 25(OH)D_3 for either the WT or *Cyp27b1*-KO mice (spleen, 7.1 ± 0.5 and 7.0 ± 0.8 ng/g; thymus, 4.6 ± 0.9 and 17.3 ± 2.0 ng/g, Fig. 2F). While the *Cyp27b1*-KO appeared to have more 25(OH)D_3 in the thymus compared to the WT, this was not a statistically significant increase. The levels of 1,25$(OH)_2D_3$ in the spleen for the WT mouse was below the LLOD (< 2 pg/g) and the *Cyp27b1*-KO was at the LLOQ (Fig. 2G). Similarly, the 1,25$(OH)_2D_3$ levels in the thymus for either mouse were also at or below the LLOQ. Taken together, data from the WT and *Cyp27b1*-KO mice confirm our expectations and/or previous data (23) that the WT kidney should contain the highest levels of 1,25$(OH)_2D_3$, the liver should be a reservoir for 25(OH)D_3, *Cyp27b1*-KO mice should have elevated 25(OH)D_3 in the kidney, and the remaining tissues would have very little to no detectable 1,25$(OH)_2D_3$.

Vitamin D metabolite profile of the M1/M21-DIKO mouse

Next, we defined the tissue metabolite levels of our experimental M1/M21-DIKO mice. These mice have a genomic deletion in enhancers that render the *Cyp27b1* gene incapable of responding to any

hormonal signals from FGF23, PTH, or $1,25(OH)_2D_3$ as well as a reduced basal expression of *Cyp27b1* (11). As mentioned, the important feature of the M1/M21-DIKO mouse is that any non-renal, inflammatory-induced response of *Cyp27b1* is unchanged from WT expression. Therefore, we hypothesize that the M1/M21-DIKO mouse is an ideal model with which to test the non-renal production of $1,25(OH)_2D_3$ in inflammation and inflammatory disease progression with the absence of renal produced $1,25(OH)_2D_3$. Since the plasma levels of vitamin D metabolites mirror that of the *Cyp27b1*-KO mouse, we expected the tissue levels of vitamin D metabolites in the M1/M21-DIKO mouse to also mirror the MSI of the *Cyp27b1*-KO mouse. In Fig. 3, we assessed the qualitative MSI profile of the M1/M21-DIKO versus the *Cyp27b1*-KO, with both mice on chow diet (3.4 IU/g vitamin D). Here, unlike Fig. 2, qualitative MS images were reconstructed using Fleximaging in contrast to the semi-quantitative evaluation performed using MSiReader software (as in Fig. 2). The intensity scale was based on total ion count using the rainbow color scale rather than the internal standard peak normalization (parula color scale) used for semi-quantitative assessment. Given this difference, these values are qualitative and not semi-quantitative (like Figs. 2 and 4). We found that in both the kidney and the liver (Fig. 3A and 3B), the M1/M21-DIKO (DIKO) mouse was comparable to the *Cyp27b1*-KO (C27KO) mouse. The $25(OH)D_3$ levels were high in the kidney tissue, and the $1,25(OH)_2D_3$ levels were low in the M1/M21-DIKO mouse. We previously found that M1/M21-DIKO mice on chow did have low, but detectable levels of $1,25(OH)_2D_3$ in the plasma compared to *Cyp27b1*-KO (11). This appears to replicate in the kidney MSI with slightly elevated levels of $1,25(OH)_2D_3$ as evidenced by increased ion intensity compared to the *Cyp27b1*-KO, however the relative quantitation was not performed. The liver contained elevated levels of $25(OH)D_3$ and no $1,25(OH)_2D_3$ metabolites.

Effect of vitamin D_3 supplementation on tissue metabolite levels in the M1/M21-DIKO mouse

Since the M1/M21-DIKO mouse lacks kidney *Cyp27b1* expression and regulation, we can exploit these features to associate vitamin D_3 supplementation of varying levels of vitamin D diets with health and disease outcomes. Therefore, we examined the tissue levels of both $25(OH)D_3$ and $1,25(OH)_2D_3$ after vitamin D_3 supplementation. We first need to rescue the mineral deficiencies of the M1/M21-DIKO mouse to recover

and maintain skeletal density and growth. Through dietary rescue with a high calcium, high phosphate, lactose containing diet, the M1/M21-DIKO mice grow to similar size and similar skeletal density to age matched WT mice (11). We found that this dietary rescue requires a minimum of 12 w of rescue diet (2% Ca, 1.25% P, 20% lactose) to recover serum Ca, P, and iFGF23 including lowering the serum PTH to WT levels (Fig. S3) and all values replicated our recent study (11). Therefore, to establish levels of vitamin D metabolites in the tissues, we first rescued mice for 12 w using the standard rescue diet (2% Ca, 1.25% P, 20% lactose containing 1.5 IU/g of vitamin D), and then switched to a diet containing either 0 IU/g of vitamin D (vitamin D deficient diet) or diet containing 20 IU/g of vitamin D daily (high D diet) for another 4 w resulting in a total experimental timeline of 16 w. We examined the extremes (0 IU and 20 IU) by MSI to capture a maximal potential effect (24). This high dietary supplementation at 20 IU was previously shown to elevate the serum levels and tissue levels of $25(OH)_2D_3$, which was our desired outcome (24). We also examined a 5 IU vitamin D_3 supplementation as a moderate dose, however given technical constraints, these mice were not examined by MSI in this study and will be examined in a future study. The mice after the additional 4 w of 0 IU or 20 IU diet were unchanged outside of femoral BMD in the female mice (Fig. S3).

In Fig. 4A and B, we examined the plasma levels of $25(OH)D_3$ and $1,25(OH)_2D_3$ by LC-MS/MS. The WT and *Cyp27b1*-KO mice (chow diet) were compared to the M1/M21-DIKO (DIKO, chow diet) mice as well as the M1/M21-DIKO mice with a 12-w rescue diet followed by 4 w either 0 or 20 IU vitamin D diet (DIKO-12wR-4w 0IU, DIKO-12wR-4w 20IU) with the full values included in Fig. S1. It is important to note that these mice were on different diets given the goals of this study: to remove circulating $1,25(OH)_2D_3$ in the M1/M21-DIKO mice and test vitamin D_3 supplementation. Rescue diets and vitamin D_3 supplementation diets for WT and *Cyp27b1*-KO mice can cause different serum vitamin D metabolite profiles (24) and will be tested in the future. In Fig. 4A, we see the M1/M21-DIKO mice on the chow diet shows a similar (not significantly different) $25(OH)D_3$ profile compared to the *Cyp27b1*-KO mouse (DIKO, 62.5 ± 4.2 ng/mL; C27KO, 77.9 ± 2.8 ng/mL, Fig. 4A). The 0 IU vitamin D diet did reduce the plasma $25(OH)D_3$ concentration in the DIKO mice (62.5 ± 4.2 ng/mL to 36.0 ± 5.7 ng/mL, Fig. 4A) and the increase of vitamin D to 20 IU raised the $25(OH)D_3$ concentration to 79.6 ± 5.1 ng/mL (Fig. 4A). The M1/M21-

DIKO mouse was on a normal chow diet (unrescued; mouse phenotype: high PTH, low Ca, P, and FGF23) for 8 weeks prior to the harvest for metabolites and these serum metabolites match our previous study (11). The M1/M21-DIKO mice were fed 12 w rescue followed by 4 w of 0 IU or 20 IU diet equaling 16 w of total diet post-wean. The $1,25(OH)_2D_3$ levels in Fig. 4B show the normal WT levels of 23.7 ± 1.9 pg/mL are greatly reduced in the *Cyp27b1*-KO, M1/M21-DIKO, and the M1/M21-DIKO with the 0 IU diet, many of which are at or below the LLOQ but above the LLOD (red data points) (3.7 ± 0.2, 5.7 ± 0.3, and 6.0 ± 0.9 pg/mL, respectively, Fig. 4B). Surprisingly, the $1,25(OH)_2D_3$ concentration in the M1/M21-DIKO mouse with the 20 IU diet was significantly increased to 17.8 ± 1.3 pg/mL (Fig. 4B), which was approaching WT levels (~ 23 pg/mL) though still significantly reduced ($p < 0.05$). These increased $1,25(OH)_2D_3$ levels could be coming from an increased production in the kidney, or perhaps from non-renal tissues, therefore we turned to the MSI in the kidney, liver, spleen, and thymus to examine this possibility.

The MSI data for the kidney, liver, spleen, and thymus is shown in Fig. 4C and 4D with the quantification listed in Fig. 4G and 4H. A complete table of the quantification and remaining representative images are shown in Fig. S1 and S2. The first and most obvious location for the increased $1,25(OH)_2D_3$ in the 20 IU diet could be from the kidney. As seen in Fig. 4C, reduction of vitamin D in the diet (0 IU) and reduction of vitamin D in the plasma (Fig. 4A), leads to a reduced amount of $25(OH)D_3$ in the kidney tissue in comparison to the 20 IU diet as evidenced by the increased ion relative intensity. The quantification of the increase is detailed in Fig. 4G where the $25(OH)D_3$ of the M1/M21-DIKO mouse with 0 IU diet is unchanged from the WT mice. However, the M1/M21-DIKO mouse with the 20 IU diet is significantly increased compared to the *Cyp27b1*-KO mouse (C27KO, 98.5 ± 6.1 ng/g; DIKO 20 IU, 174.0 ± 14.4 ng/g, Fig. 4G). Despite this increase in the $25(OH)D_3$ levels, it did not appear to cause any increased $1,25(OH)_2D_3$ production in the kidney of the M1/M21-DIKO mouse on the 20 IU diet. The MSI images (Fig. 4C, lower) show little to no presence of $1,25(OH)_2D_3$ and the quantification in Fig. 4H demonstrates that the M1/M21-DIKO mice with either 0 IU or 20 IU diet are below the LLOQ yet above the LLOD, equivalent to the *Cyp27b1*-KO mice (C27KO, 3.8 ± 0.4 pg/g; DIKO 0 IU, 5.3 ± 0.6 pg/g; DIKO 20 IU, 5.6 ± 0.7 pg/g, Fig.

4H). It would appear from these data that the source of the increased $1,25(OH)_2D_3$ in the plasma is not derived from the kidney.

The reservoir of $25(OH)D_3$ in the liver of the WT and *Cyp27b1*-KO mice is reduced in the M1/M21-DIKO mice on the 0 IU diet (WT, 202.5 ± 13.9 ng/g; C27KO, 212.7 ± 11.6 ng/g; DIKO 0 IU, 95.3 ± 5.3 ng/g, Fig. 4G), and is markedly increased in the M1/M21-DIKO mice on the 20 IU diet (287.5 ± 13.7). The WT, *Cyp27b1*-KO, and M1/M21-DIKO 0 IU all have $1,25(OH)_2D_3$ levels at or below the LLOQ, however, the M1/M21-DIKO 20 IU diet shows an increase in $1,25(OH)_2D_3$ levels (18.4 ± 5.4 pg/g, Fig. 4H). While these biological replicates are variable, they were significantly increased and the MSI images for the $1,25(OH)_2D_3$ showed very punctate regions of higher ion intensity. The spleen and thymus both show lower levels of $25(OH)D_3$ that are at or below the LLOQ and both tissues have an elevation of $25(OH)D_3$ in the M1/M21-DIKO mice on the 20 IU diet. Unlike the modest elevations in the $25(OH)D_3$, the spleen had significant increases in $1,25(OH)_2D_3$ in both M1/M21-DIKO dietary samples (WT, <LLOD; C27KO, 5.4 ± 0.8 pg/g; DIKO 0 IU, 16.3 ± 2.3 pg/g; DIKO 20 IU, 57.8 ± 4.7 pg/g, Fig. 4H) and the MSI images depict a broad elevation of ion intensity of metabolite across the tissue. In Fig. 4I, we examined the spatial features of MSI. The splenic data (from Fig. 4E) was overlaid with an H&E staining of a section taken immediately following the MSI tissue section. We found that while $25(OH)D_3$ was rather broadly increased, it appears that the $1,25(OH)_2D_3$ intensity increases in the white pulp segments of the thymus which are rich in T cells and macrophages that encompass the periarteriolar sheaths, follicles, and marginal zones (25). Finally, $1,25(OH)_2D_3$ in the thymus was also increased modestly with DIKO 20 IU diet (WT, 5.5 ± 0.9 pg/g; DIKO 20 IU, 16.9 ± 1.7 pg/g, Fig. 4H). These data indicate that these non-renal tissues, and possibly others not examined, are both 1) transporting $25(OH)_2D_3$ into these tissues and 2) may be leading to the elevation of $1,25(OH)_2D_3$ detected in the plasma by LC-MS/MS analysis (Fig. 4B).

To confirm the validity of the MSI relative quantitation data for each of these tissues, we conducted an important homogenate analysis of the remaining tissue block by LC-MS/MS absolute quantitation. We processed the *Cyp27b1*-KO (chow), M1/M21-DIKO (0 IU and 20 IU rescue diet) samples for this confirmation as described in the Methods. $25(OH)D_3$ levels from the tissue homogenate mirrored those

from the MSI data analysis (Fig. 5A, example: C27KO – MSI, 98.5 ± 6.1 ng/g vs Tissue Homogenate, 95.3 ± 9.4 ng/g, remaining data found in Fig. S1). Similarly, data for $1,25(OH)_2D_3$ (Fig. 5B) corroborate their MSI counterparts well thus confirming the validity of the MSI data. In further validation of the method, a Bland-Altman analysis was performed (examples shown in Fig. S4) (26). Despite the limited n values (n=3), this analysis showed an average bias of 1.013 ± 0.121 and the 95% Limits of Agreement ranged from 0.85 ± 0.06 to 1.21 ± 0.12 across each grouping of samples between the methods indicating that these methods are highly comparable.

Gene expression consequences of elevated tissue $1,25(OH)_2D_3$

With elevated $1,25(OH)_2D_3$ expression in tissues, we hypothesized that perhaps these tissues would have elevated levels of vitamin D target genes. We first confirmed the elevation of megalin and cubulin expression in the kidney versus non-renal tissues (Fig. S5). In Fig. S5, there is 100-fold more megalin (*Lrp2*) and cubulin (*Cubn*) found in the kidney, so $25(OH)D_3$ availability may be the highest. Furthermore, for these target genes to be responsive to $1,25(OH)_2D_3$, the tissue should have expression of the vitamin D receptor (VDR). Therefore, we also evaluated the levels of *Vdr* expression in each of the tissues examined by MSI and in the M1/M21-DIKO mice that were fed either the 12-w rescue diet followed by 4 w of 0 IU or 20 IU diet. As can be seen in Fig. 6A, the kidney had the highest expression of *Vdr,* and this expression was increased with the feeding of the 20 IU diet. The liver was 100-fold lower expression than the kidney and the spleen and thymus were both 10-fold lower and unchanged in either diet condition. We next wanted to assess the downstream consequences of higher $1,25(OH)_2D_3$ production in the tissues by looking at the target gene of *Cyp24a1*, one of the most sensitive vitamin D target genes. As can be seen in Fig. 6B, the kidney retained the highest level of *Cyp24a1* expression that was increased by the 20 IU diet. The remaining tissues were 1000-fold lower in expression and were unchanged by diet. The expression of *Cyp24a1* was at the threshold of detection by qPCR analysis in all tissues outside of the kidney in the absence of exogenous $1,25(OH)_2D_3$ (9). It appeared that either the elevated plasma levels of $1,25(OH)_2D_3$ in the 20 IU diet (Fig. 4B and S1) may be causing an elevation of *Cyp24a1* and *Vdr* in the kidney, or the retention of

$25(OH)D_3$ in the kidney has reached levels high enough to activate the VDR directly to increase both *Cyp24a1* and *Vdr* (24, 27-29). The expression of *Cyp27b1* was unchanged in any diet condition (data not shown).

If the hypothesis of localized $1,25(OH)_2D_3$ production affecting the inflammatory program of the immune cells is true, then we may see differential regulation of cytokines involved in pro- and anti-inflammatory responses (2, 30). In Fig. 6C, we examined the gene expression of several anti-inflammatory cytokines (*Il4*, *Il10*) and pro-inflammatory cytokines (*Tnfa, Il17b, Il6*, and *Il1b*) in the spleen, which was the tissue with the highest $1,25(OH)_2D_3$ concentration demonstrated by both MSI and confirmatory tissue homogenate. $1,25(OH)_2D_3$ has been shown to suppress the proinflammatory cytokines like *Tnfa* and *Il17b* and increase anti-inflammatory cytokines like *Il4* and *Il10* in macrophages and T cells during polarization, inflammatory disease, and cell differentiation (31-34). We found that *Il4* was significantly increased in the spleen, whereas *Tnfa* was suppressed. The remaining cytokines were not statistically changed. These data demonstrate a potential outcome of the production of $1,25(OH)_2D_3$ in the spleen.

Discussion

The landmark finding of this study is the detection and measurement of non-renal vitamin D metabolite production in the absence of circulating $1,25(OH)_2D_3$. This was only made possible by using our M1/M21-DIKO animal and its unique phenotype that mirrors the *Cyp27b1*-KO while retaining a mature CYP27B1 protein (all tissues) and non-renal inflammatory induction of *Cyp27b1* (11). A human study of anephric patients was recently published that corroborate our findings on the potential for non-renal $1,25(OH)_2D_3$ production in the absence of kidney $1,25(OH)_2D_3$ production (17). Our unique animal model gives us the flexibility to manipulate dietary conditions, model different diseases, and isolate tissues for direct measurements. Here, we isolated the ability of vitamin D_3 supplementation to elevate tissue distribution of both $25(OH)D_3$ and $1,25(OH)_2D_3$ in the animal and assess the downstream consequences after our dietary rescue. Using our targeted-metabolite MSI platform, we were able to identify and confirm tissue distribution of $25(OH)D_3$ and $1,25(OH)_2D_3$ in the wildtype mice and the control animal, the *Cyp27b1*-KO

mouse. Interestingly, the relative quantitation revealed that the WT mouse contained approximately 3-fold higher levels of $1,25(OH)_2D_3$ in the tissue (66.4 ± 3.4 pg/g, Fig. 4H and S1) compared to $1,25(OH)_2D_3$ measured in the plasma (23.7 ± 1.9 pg/mL, Fig. 4B and S1). The $25(OH)D_3$ levels on the other hand were also elevated in the kidney tissue (34.1 ± 3.1 ng/g. Fig. 4A and S1) versus the plasma measurements (15.4 ± 1.1 ng/mL, Fig. 4G and S1). This provides an interesting observation and perhaps avenue to explore the export of $1,25(OH)_2D_3$ from the tissue into the plasma, or it may be a consequence of the degradation of $1,25(OH)_2D_3$ (or $25(OH)D_3$) to $1,24,25(OH)_2D_3$ (or $24,25(OH)_2D_3$) prior to exit from the tissue. $1,24,25(OH)_2D_3$ and $24,25(OH)_2D_3$ were not measured in this study but are a focus for future experiments.

Outside of the kidney, we expected the liver to be a repository of $25(OH)D_3$ and it was, with levels that were again quite elevated from the plasma (35, 36). The thymus and spleen had very little $25(OH)D_3$ and levels of $1,25(OH)_2D_3$ (Fig. 4) that were at or below the LLOQ or LLOD on a diet with normal vitamin D levels, which was our expectation. The *Cyp27b1*-KO mice were an excellent control and recapitulated the expectations from the plasma analysis of vitamin D metabolites. The *Cyp27b1*-KO mice are known to have elevated levels of $25(OH)D_3$ and this was apparent in both in the liver and kidney tissues (10). This elevation is due to two phenomena: 1) inactivation of the CYP27B1 enzyme, thus no conversion, and more importantly, 2) secondary hyperparathyroidism that suppresses the activity and expression of the *Cyp24a1* gene and CYP24A1 enzyme (9, 11). The levels of $1,25(OH)_2D_3$ are 1000-fold less than $25(OH)D_3$ in the plasma (picograms vs nanograms) and thus the driving force behind the substrate excess is likely more due to this suppression of *Cyp24a1* and the degradation of $25(OH)D_3$ to $24,25(OH)_2D_3$. Our previous studies show that when PTH levels are high, there is very little conversion to $24,25(OH)_2D_3$ (9-11). The MSI captures these features faithfully to previous observations as well as highlighting the fact that while plasma levels of $1,25(OH)_2D_3$ are easiest to measure clinically, the tissue levels appear to be a significant variable and may vary widely in patient populations. Additionally, the ratios of $25(OH)D_3$ to not only $24,25(OH)_2D_3$ but also to the production of the $25(OH)D_3$-26,23-lactone, a metabolite that is in less flux than $24,25(OH)_2D_3$, are more valuable to determine output of vitamin D metabolism in clinical patients (37-39). These additional metabolites will be examined in future studies.

Based on our previous skeletal rescue in the M1/M21-DIKO mice (11), we chose to first establish a rescued animal in both the skeleton and PTH levels in the plasma prior to changing the vitamin D levels in the diet. We had previously optimized this diet for skeletal rescue over a minimum of 12 w (11). We then changed the diet for an additional 4 w with varying levels of vitamin D_3 supplementation, selecting the 0 IU diet and 20 IU diet as the extremes. We chose the 20 IU diet based on prior studies that demonstrated increased $25(OH)D_3$ availability in tissues and high elevation of serum $25(OH)D_3$ after 12 w of feeding (24) to ensure transport differences in the tissues, based on megalin/cubulin expression, were overcome to deliver $25(OH)D_3$ into the non-renal tissues. At the 4-w time point, the mice on the 0 IU diet are not completely vitamin D "deficient" as evidenced by the plasma levels of $25(OH)D_3$ measured (Fig. S1), however with extended feeding of this diet we have achieved plasma $25(OH)D_3$ levels below the LLOD by LC-MS/MS absolute quantitation (data not shown). The 0 IU diet does achieve the stated purpose for our study at 4 w, as the MSI shows that tissue levels are greatly depleted of $25(OH)D_3$ in the kidney (Fig. 3 - M1/M21-DIKO and Fig. 4 - 0 IU diet). Elevation of vitamin D_3 in the diet to 20 IU/g, increases the $25(OH)D_3$ in the plasma, liver, and kidney. This elevation though, did not lead to any more $1,25(OH)_2D_3$ being made in the kidney of the M1/M21-DIKO mouse. Importantly, now we find $25(OH)D_3$ by MSI in the spleen and modestly in the thymus, providing the substrate for potential conversion to $1,25(OH)_2D_3$. In turn, we found that the $1,25(OH)_2D_3$ in the spleen was elevated to levels that rivaled the WT kidney tissue (spleen 20 IU, 57.8 ± 4.7 pg/g; kidney WT, 66.4 ± 3.4 pg/g, Fig. 4). It is possible then that the spleen is contributing to the elevated plasma levels of $1,25(OH)_2D_3$ that are found in the M1/M21-DIKO mice on the 20 IU diet, however, there are many other tissues that may also be contributing in a similar manner that were not analyzed by MSI in this study such as the parathyroid, skin, or intestinal tissues.

We also found the elevation in liver $1,25(OH)_2D_3$ an intriguing result (Fig. 4). The MSI shows punctate regions of increased ion intensity. The resolution of MSI does not yet allow cellular resolution but it is possible that there are small cell populations like stellate cells or infiltrated macrophages resident in the liver that are causing these punctate ion intensity signals (40, 41). As mentioned, the current resolution of MSI is near 35 μm in size, thus ablating ~3-5 cells at a time, so this method is incapable of individual cell

resolution. Similarly, the apparent low expression of *Cyp27b1* in non-renal tissues could be adequate expression in a select subpopulation of cells surrounded by a high-abundance, homogenous mix of non-expressing cells. Other projects in the lab are focused on the discovery of these subpopulations. Finally, we are not proposing the 20 IU diet as a human clinical dietary intervention, it was chosen to portray a "high" or "maximal" effect in these studies to validate the MSI technique and dietary differences. Now that we have established this vital linkage between supplementation and non-renal production of calcitriol, we will examine different vitamin D_3 supplementation levels in diets and their outcome not only in MSI, but also for inflammatory disease amelioration in M1/M21-DIKO, WT, and additional genotypes.

The power of MSI is in visualizing the spatial distribution of these vitamin D metabolites within the tissue themselves, in addition to the metabolite relative quantitation. We saw in Fig. 2A and from the schematic in Fig. 2E and extrapolating that to the Fig. 2A panels, that the $25(OH)D_3$ appeared to be focused in the kidney cortex and outer medulla, whereas $1,25(OH)_2D_3$ appeared across the cortex, outer medulla, and inner medulla, with the highest intensity apparent at the inner medulla. We find it interesting that $1,25(OH)_2D_3$ has a higher intensity in what appears to be a different location than peak $25(OH)D_3$ intensity. Our previous genomic data indicate there was an obvious tissue specific isolation of the *Cyp27b1* enhancers to the proximal convoluted tubule cells (8). While these data are intriguing, we do not understand these distributions and why it appears the locations differ between the substrate and product. It is possible that some of this can be explained by the inevitable diffusion of metabolites during the OTCD processing and thus a technical aberration (23). It also highlights the need for continued development and experimentation in this powerful platform. Despite this, the MSI technique is clearly a methodology that can be used to study the transport of these vitamin D metabolites from tissues. For the spleen in Fig. 4I, we found that the $25(OH)D_3$ is widely distributed, but the $1,25(OH)_2D_3$ appears to have higher relative ion intensity in what appear to be the germinal centers and perhaps the marginal zones within the white pulp of the spleen (42). These areas contain higher concentrations of B cells under development and macrophages. Macrophages are one cell type that has been known to generate $1,25(OH)_2D_3$ in an inflammatory disease state (12, 43, 44). We are now focused on refining this resolution and limiting diffusion to focus on specific structures,

cell populations, and regions of interest. One such application will be in defining the contributions of vitamin D metabolites in immune cells or others at the point of disease contact in areas such as colonic or atherosclerotic lesions. While $25(OH)D_3$ and $1,25(OH)_2D_3$ are important to identify, we are also focused on expanding this technique to capture the catabolic derivatives of these metabolites in $24,25(OH)D_3$ and $1,24,25(OH)D_3$ and others. We, and others, have demonstrated relationships between metabolites such as $25(OH)D_3$ and $24,25(OH)D_3$ that can be predictive on PTH levels and skeletal health (37, 45, 46). As we expand our studies to disease models, we will explore the ratios of $25(OH)D_3$:$24,25(OH)_2D_3$ and $25(OH)D_3$:$25(OH)D_3$-26,23-lactone in tissues compared to the plasma.

In the final set of experiments, we looked at the impact of $1,25(OH)_2D_3$ production in the tissues on gene expression. For $1,25(OH)_2D_3$ to have a consequence, the VDR should be expressed in these tissues. We confirmed previous studies (10, 11) for the concentrations of *Vdr* expressed in the tissues we isolated in that kidney was the highest, followed by thymus and spleen, with the liver having very low levels of *Vdr* detected by qPCR (Fig. 6). We also confirmed that *Cyp24a1* expression was very low in these non-renal tissues, often at the threshold of detection by qPCR analysis. *Cyp24a1* was not elevated in these tissues after high vitamin D_3 supplementation facing physiologic levels of $1,25(OH)_2D_3$. We have found that supraphysiologic injections of $1,25(OH)_2D_3$ easily activate the *Cyp24a1* gene in any tissue that contains the VDR (10, 11). This is different than the activities in the kidney post 20 IU vitamin D_3 supplementation. Here in the kidney, the physiologic elevations in $1,25(OH)_2D_3$ lead to activation of *Cyp24a1*. We believe that this indicates two different modes for *Cyp24a1* activity in the body: 1) renal regulation of *Cyp24a1* responds to and maintains the circulating blood $1,25(OH)_2D_3$ levels, and 2) non-renal *Cyp24a1* exists for emergency detoxifying circumstances. When faced with physiologic levels of $1,25(OH)_2D_3$, those non-renal tissues preserve $1,25(OH)_2D_3$ for positive gene expression (no *Cyp24a1* expressed), when exposed to higher levels of $1,25(OH)_2D_3$, the detoxification program is initiated in all tissues. If vitamin D is anti-inflammatory as the literature would suggest, we should see consequences of these $1,25(OH)_2D_3$ changes in immune cells and in tissues that harbor immune cells like the spleen (2, 31, 34, 47). We did, in fact, see a change in both *Tnfa* and *Il4* in the spleen. These cytokines were unchanged in the liver and thymus (data

not shown). In prior studies with *Cyp27b1*-KO mice, it was found that the 20 IU vitamin D_3 dietary supplementation fed for 12 weeks was able to induce gene expression in the intestine (24). While we used a shorter term for vitamin D_3 supplementation (4 w), and we found very little $25(OH)D_3$ in tissues outside of the kidney and liver, it is still possible these elevated levels of $25(OH)D_3$ are causing gene regulation in the spleen. $25(OH)_2D_3$-actived VDR is very difficult to control for experimentally in the animal, therefore, we will continue to examine these diets at varying vitamin D_3 concentrations to help clarify $25(OH)D_3$-activated VDR expression. Given our gene expression results in the spleen, it appears this elevation of splenic $1,25(OH)_2D_3$ may affect the immune program. We are currently focused on isolation of different immune populations for closer examination of their expression and differentiation under these dietary conditions. We are also examining these cell populations in inflammatory disease models for their contribution to amelioration of disease.

In conclusion, this work is the first example of leveraging the power of the OTCD-MALDI-MSI platform to capture and quantify the renal and non-renal production of vitamin D metabolites. We can manipulate the plasma levels of $25(OH)D_3$ through vitamin D_3 supplementation, not $1,25(OH)_2D_3$ or $25(OH)D_3$ dosing, and this appears to have consequences to gene expression and production of $1,25(OH)_2D_3$. Continued development of this platform will enable us to identify the connection between plasma vitamin D levels, or status, and disease benefits that we believe will help guide future clinical recommendations.

Methods

Sex as a biological variable: For all studies, both male and female mice were included in the analyses. Sex was considered as a biological variable and data were reported as mixed where no differences were found in the data.

Materials: 1α,25$(OH)_2D_3$, acetone, hexane, zinc sulphate, gelatine, 2-mercaptobenzotiazole (MBT) and sodium borohydride we purchased from Sigma-Aldrich (UK). 25$(OH)D_3$, commercially available lyophilized four-point calibration standards were purchased from (Chromsystem, München, GmBH). Amplifex® Dieen reagent was purchased from Sciex (Chemistry and Consumables R&D, Framingham, MA, US). Isotopically labelled d6-25$(OH)D_3$ and d6-1α,25$(OH)_2D_3$ were purchased from Cambridge Isotope Laboratories (MA, US). 25$(OH)D_3$ serum calibrators were purchased from Chromsystem GmbH. LC-MS grade acetonitrile (ACN), methanol and formic acid were obtained from Fisher (UK). The water used was generated through a direct-Q Ultrapure water system from Millipore (Bedford, MA) with a specific resistance of 18.2 MΩ cm. Traditional genotyping PCR was completed with GoTaq (Promega, Madison, WI) and all real-time qPCR was completed with the StepOnePlus using TaqMan for gene expression assays (Applied Biosystems, Foster City, CA). Primers were obtained from IDT (Coralville, IA).

Animal Studies: All mice were derived from or created in the C57BL/6J genetic background as previously described (10, 11). *Cyp27b1*-KO, M1/M21-DIKO, and littermate wildtype (WT) mice aged 8-9 w (The Jackson Laboratory, Bar Harbor, ME) were housed in high density ventilated caging in the Biochemistry Animal Research Facility of the University of Wisconsin-Madison under 12-hour light/dark cycles at 72°F and 45% humidity. Mice used in this study were maintained on a standard rodent chow diet (5008, Lab Diet, St. Louis, MO), rescue diet (1.5 IU vit D/g, 2% Ca, 1.25% P, 20% lactose, TD.96348, Inotiv/Envigo, Madison, WI), 0 IU diet (0 IU vit D/g, 2% Ca, 1.25% P, 20% lactose, TD.200097, Inotiv/Envigo, Madison, WI), or 20 IU diet (20 IU vit D/g, 2% Ca, 1.25% P, 20% lactose, TD.200096, Inotiv/Envigo, Madison, WI). M1/M21-DIKO mice were fed the rescue diet for 12 w post-wean, followed by a diet switch to either the 0 IU or 20 IU diet for an additional 4 w (16 w total diet, mouse aged 19 w). All animal studies were reviewed and approved by the Research Animal Care and Use Committee of University of Wisconsin-Madison under protocol A005478. Unless otherwise indicated, all experiments were conducted with equal numbers of males and females ($n \geq 6$). From these mice, a subset was chosen for MSI ($n = 3$) for each diet and genotype

condition, including both M and F in the groups. MSI is a technically complex method which is not easily scaled to high n value experiments. We determined that n=3 provided statistically sound data for this study. Data were reported as mixed, as no differences were found between the sexes.

Tissue perfusion and collection: Mice were anesthetized under ether, opened, and blood was collected by cardiac puncture and split into serum or EDTA-treated plasma. Post puncture 10 mL of 1x PBS was perfused to remove blood from the circulation and tissues. Intratissue systemic contribution of blood in all target tissues was assessed by monitoring the heme b ion from myoglobin containing an iron ion in the +3 oxidation state as (Fe(III) + porphyrin ($C_{34}H_{32}N_4O_4Fe_1$))+ at m/z 616.1772 ± 0.025 Da. No systemic contribution was observed for all tissues as signal/noise (S/N) of the heme b ion was below 3. For MSI, tissues were dissected, weighed, and drop frozen in liquid N_2 in 2.0 mL cryo vials. For gene expression, tissues were dissected and drop frozen in liquid N_2 in microfuge tubes. All tissues were stored long term in -80°C.

Blood Chemistry: Cardiac blood was collected at the time of sacrifice. Collected blood was split into serum or EDTA-treated plasma, incubated at room temperature for 30 min followed by centrifugation at 6,000 rpm for 12 min (x2) to obtain serum or EDTA-plasma (10). Serum calcium and phosphate levels were measured using QuantiChrom™ Calcium Assay Kit (#DICA-500, BioAssay Systems, Hayward, CA) and QuantiChrom™ Phosphate Assay Kit (#DIPI-500, BioAssay Systems, Hayward, CA) (10). Circulating intact FGF23 and PTH were measured in EDTA plasma via a Mouse/Rat FGF-23 (Intact) ELISA Kit (#60-6800, Immutopics, San Clemente, CA) and a Mouse PTH (1-84) ELISA kit (#60-2305, Immutopics), respectively (10).

Bone Mineral Density (BMD): BMDs were measured and analyzed by dual x-ray absorptiometry (DEXA) with a PIXImus2 densitometer (GE-Lunar Corp, Madison, WI) as previously described (48).

Gene Expression: Frozen tissues were homogenized in Trizol Reagent (Life Technologies) and RNA was isolated as per the manufacturer's instructions. 1 µg of isolated total RNA was DNase treated, reverse transcribed using the High-Capacity cDNA Kit (Applied Biosystems), and then diluted to 100 µL with RNase/DNase free water. qPCR was performed using primers specific to a select set of differentially expressed genes by TaqMan analyses. TaqMan Gene Expression probes (Applied Biosystems) used in Supplemental Table 1.

Tissue Sectioning and Mounting: Tissue preparation Sectioning was performed on frozen target tissues from each mouse using a Leica cryostat (CM 1850 UV; Leica Biosystems, Nußloch, Germany) with gelatine (10% v/v) as a mounting medium. Adjacent cross Sects. (12 µm thickness) were taken from a top-down (horizontal) plane and thaw-mounted onto conductive indium tin oxide (ITO)–coated slides (Bruker Daltonik, Bremen, GmBH & CO. KG). Further adjacent Sects. (10 µm thickness) were mounted onto a slide pre-coated with poly-l-lysine for histological staining. The remaining tissue was used for tissue homogenate analysis by LC-MS/MS. All sections were dried in a vacuum desiccator at room temperature for 30 min and stored at − 80 °C for analysis.

Instrumentation: MSI experiments were performed on an Orbitrap® LTX-XL Mass Spectrometer (Thermo Fisher Scientific, GmbH, Bremen Germany) couple to a reduced pressure ESI/MALDI interface (Spectroglyph LLC, Kennewick, US). Confirmatory Liquid Chromatography-Tandem Mass Spectrometry analysis was performed using a triple-quadrupole linear Ion trap Mass Spectrometer SCIEX 5500+ Qtrap (Sciex, Framingham, US) couple with an Ultra high pressure Liquid Chromatography system Nexera® UPLC (Shimadzu, Kyoto, Japan).

On-Tissue Chemical Derivatization (OTCD): At -80 °C, tissue sections were dried in a vacuum desiccator (20 min). Amplifex reagent (5 mL, 0.1 mg/mL in 50:50 v/v acetonitrile/water) was applied to the tissue sections by protocol adapted from (23) using an artistic airbrush (AirFlow, SZ, China) instead of an

automated Image Prep due to restricted quantities of Ampiflex® reagent. Briefly, a reagent solution of Amplifex (2 mL, 0.25 mg/mL in 50:50 v/v acetonitrile/water) with the incorporation of 10µL of ITSD (d6-25(OH)D3 at 1ng/ml was sprayed positioned 20 cm away from the target with a N_2 pressure of 1.2 bar. 2 ml/slide with each manual pass of approx. 1 s and repeated with 5-10 s between passes until uniform coating was achieved (ϱ of 0.015 mg/cm^2). Then, the slide was placed in a closed reaction container, containing a 1:1 v/v solution of acetonitrile/water and a moist Kimwipe under the lid and placed in an oven at 37 °C for 1 h for derivatization completion. Sections were then dried under vacuum desiccator (25min) and ready for MALDI matrix application.

Matrix Application: Matrix Application 2-mercaptobenzothiazole (10 mL, 6 mg/mL in 90:10 v/v acetonitrile/water) was applied in eight passes using a 3D printer, as previously described(23, 49). A flow rate of 0.1 mL/min with a gas pressure of 2 bar, a bed temperature of 30 °C, a z-height of 30 mm, and a velocity of 1100 mm/min were achieved, averaging a run time of 30 min per slide. A uniform coating of matrix was achieved with 0.12 mg/cm^2.

Mass Spectrometry Imaging Acquisition: MSI experiments were performed on an Orbitrap LTQ-XL Mass Spectrometer (Thermo Fisher Scientific, GmbH, Bremen, Germany) couple with a reduced pressure Electrospray (ESI)/MALDI interface (Spectroglyph, Kennewick, WA, US). Further details on the interface can be found in Belov et al., 2017(50). The 349nm MALDI laser (Spectra Physics, MV, CA, US) was operated at a repetition rate of 1000Hz and pulse energy of ~2.3µJ. The Mass Spectrometer was operated in positive ion mode using a maximum ion injection time of 250ms in FT mode, automatic gain control (ACG) turned off and a mass range of 500-800Da.The spectral resolution was set to 60.000FWHM at *m/z* 400. The experiments were performed at 100x100 µm spatial resolution for liver and thymus tissue sections and 75x75 µm for kidney and spleen tissue sections. Optical images were taken using a flatbed scanner (Cannon LiDE-20, Cannon, UK). The instrument was calibrated using ESI Cal mix solution as per manufacture specifications. Collision induces dissociation experiments (CID) on both VitD metabolites

($1\alpha,25(OH)_2D_3$ and $25(OH)D_3$ Ampiflex derivatives was performed for structural confirmatory analysis at corresponding precursor masses *m/z* 732.50 and *m/z* 748.50 with an isolation window of 2 Da summing 10 scans/spectra using 16 and 17 V as collision energies (CE) respectively covering a scan range of 280-750Da.

Spectra Processing: Thermo Fisher raw data were aligned to the corresponding position files in Image Insight software (Spectroglyph, Kennewick, WA, US) and exported form there as ImzML files using the supplier recommended default parameters. The ImzML files were uploaded onto the open-source MSiReader version 1.02 9 (Raleigh, NC, US) using MATLAB version 2022b and Fleximaging version 5.1 (Bruker Daltonik, GmBH). All data was normalized using the d6-$25(OH)D_3$ mass at (M^+) 738.5435± 0.025Da (peak normalization). MS images were generated for both vitamin D metabolites detected as Ampiflex derivatives at *m/z* 732.5058±0.025 for $25(OH)D_3$ and *m/z* 748.5008±0.025 for $1\alpha,25(OH)_2D_3$. For relative semi-quantitation (tissue mimetic model), intensities values for each metabolite as Ampiflex® derivatives were collected and ratios calculations against the ISTD (d6-25(OH)D3 were calculated. Relative quantitation was accomplished by plotting ratio intensities against matrix-matched standard calibration using the mimetic model. MSiQuant (part of the MSiReader software package) was used as software for calculations.

Confirmatory LC-MS/MS analysis (absolute quantitation): Please see supplementary methods.

Histological Staining: Please see supplementary methods.

Statistical Analysis: Data were analyzed using GraphPad Prism 10.2.2 software (GraphPad Software, Inc., La Jolla, CA) and in consultation with the University of Wisconsin Statistics Department. All values are reported as the mean ± standard error (SEM) and differences between group means were evaluated using One-Way ANOVA or Student's *t*-test (1-tailed) as indicated in the figure legends. Bland-Altman was

performed in Graphpad Prism. Significance is determined by p-values with $p < 0.05$ and p values are reported in each figure and figure legend (*, $p<0.05$; **, $p<0.01$; ***, $p<0.001$; ****, $p<0.0001$).

Study approval: All animal studies were reviewed and approved by the Research Animal Care and Use Committee of University of Wisconsin-Madison under protocol A005478.

Data availability: Values for all data points and graphs for this study are reported in the Supporting Data Values file and are included in the supplemental materials. All images used and replicates are available in the supplemental materials. Data from MSI studies were processed using MSiQuant software from the MSiReader Software Package and compiled in Excel and GraphPad Prism.

Author contributions: Conceptualization, M.B.M, J.W.P, D.F.C; Investigation, M.B.M, S.M.L, S.R.C, D.F.C.; Writing – Original Draft, M.B.M., D.F.C; Writing – Review & Editing, M.B.M, S.M.L, S.R.C, J.W.P, D.F.C; Data Curation, M.B.M.

Acknowledgements: We thank members of the Meyer Laboratory for their contributions during manuscript preparation.

Funding: Our funding was provided by the National Institutes of Health grants HL159645 to M.B.M. and DK117475 to J.W.P. The content is solely the responsibility of the authors and does not necessarily represent the official views of the National Institutes of Health.

FOOTNOTES

Abbreviations used: $1,25(OH)_2D_3$, 1,25 dihydroxy vitamin D; FGF23, fibroblast growth factor 23; PTH, parathyroid hormone; Ca, calcium; P, phosphate; M1, *Mettl1* intronic enhancer of *Cyp27b1*; M21, *Mettl21b* intronic enhancer of *Cyp27b1*; M1/M21-DIKO, M1 and M21 double intronic enhancer knockout

out; Mass Spectrometry Imaging (MSI); LC-MS/MS, high pressure liquid chromatography – tandem mass spectrometry; On-tissue chemical derivatization (OTCD). Matrix Assisted Laser Desorption Ionization (MALDI)

References

1. DeLuca HF. Overview of general physiologic features and functions of vitamin D. *Am J Clin Nutr.* 2004;80(6 Suppl):1689S-96S.
2. Cantorna MT, Snyder L, Lin YD, and Yang L. Vitamin D and 1,25(OH)2D regulation of T cells. *Nutrients.* 2015;7(4):3011-21.
3. Yang L, Weaver V, Smith JP, Bingaman S, Hartman TJ, and Cantorna MT. Therapeutic effect of vitamin d supplementation in a pilot study of Crohn's patients. *Clin Transl Gastroenterol.* 2013;4(4):e33.
4. Froicu M, and Cantorna MT. Vitamin D and the vitamin D receptor are critical for control of the innate immune response to colonic injury. *BMC Immunol.* 2007;8:5.
5. Hahn J, Cook NR, Alexander EK, Friedman S, Walter J, Bubes V, et al. Vitamin D and marine omega 3 fatty acid supplementation and incident autoimmune disease: VITAL randomized controlled trial. *BMJ.* 2022;376:e066452.
6. Manson JE, Cook NR, Lee IM, Christen W, Bassuk SS, Mora S, et al. Vitamin D Supplements and Prevention of Cancer and Cardiovascular Disease. *N Engl J Med.* 2019;380(1):33-44.
7. Fuleihan Gl-H, Bouillon R, Clarke B, Chakhtoura M, Cooper C, McClung M, et al. Serum 25-Hydroxyvitamin D Levels: Variability, Knowledge Gaps, and the Concept of a Desirable Range. *J Bone Miner Res.* 2015;30(7):1119-33.
8. Meyer MB, and Pike JW. Genomic mechanisms controlling renal vitamin D metabolism. *J Steroid Biochem Mol Biol.* 2023;228:106252.

9. Meyer MB, Lee SM, Carlson AH, Benkusky NA, Kaufmann M, Jones G, et al. A chromatin-based mechanism controls differential regulation of the cytochrome P450 gene *Cyp24a1* in renal and nonrenal tissues. *J Biol Chem.* 2019;294(39):14467-81.

10. Meyer MB, Benkusky NA, Kaufmann M, Lee SM, Onal M, Jones G, et al. A kidney-specific genetic control module in mice governs endocrine regulation of the cytochrome P450 gene *Cyp27b1* essential for vitamin D_3 activation. *J Biol Chem.* 2017;292(42):17541-58.

11. Meyer MB, Benkusky NA, Kaufmann M, Lee SM, Redfield RR, Jones G, et al. Targeted genomic deletions identify diverse enhancer functions and generate a kidney-specific, endocrine-deficient *Cyp27b1* pseudo-null mouse. *J Biol Chem.* 2019;294(24):9518-35.

12. Adams JS, Singer FR, Gacad MA, Sharma OP, Hayes MJ, Vouros P, et al. Isolation and structural identification of 1,25-dihydroxyvitamin D3 produced by cultured alveolar macrophages in sarcoidosis. *J Clin Endocrinol Metab.* 1985;60(5):960-6.

13. Nykjaer A, Fyfe JC, Kozyraki R, Leheste JR, Jacobsen C, Nielsen MS, et al. Cubilin dysfunction causes abnormal metabolism of the steroid hormone 25(OH) vitamin D(3). *Proc Natl Acad Sci U S A.* 2001;98(24):13895-900.

14. Leheste JR, Rolinski B, Vorum H, Hilpert J, Nykjaer A, Jacobsen C, et al. Megalin knockout mice as an animal model of low molecular weight proteinuria. *Am J Pathol.* 1999;155(4):1361-70.

15. Nykjaer A, Dragun D, Walther D, Vorum H, Jacobsen C, Herz J, et al. An endocytic pathway essential for renal uptake and activation of the steroid 25-(OH) vitamin D3. *Cell.* 1999;96(4):507-15.

16. Bikle D, Bouillon R, Thadhani R, and Schoenmakers I. Vitamin D metabolites in captivity? Should we measure free or total 25(OH)D to assess vitamin D status? *J Steroid Biochem Mol Biol.* 2017;173:105-16.

17. Jørgensen HS, de Loor H, Billen J, Peersman N, Vermeersch P, Heijboer AC, et al. Vitamin D Metabolites Before and After Kidney Transplantation in Patients Who Are Anephric. *Am J Kidney Dis.* 2024.

18. Meyer MB, Benkusky NA, Lee SM, Yoon SH, Mannstadt M, Wein MN, et al. Rapid genomic changes by mineralotropic hormones and kinase SIK inhibition drive coordinated renal Cyp27b1 and Cyp24a1 expression via CREB modules. *J Biol Chem.* 2022:102559.

19. Miller BE, and Norman AW. Enzyme-linked immunoabsorbent assay (ELISA) and radioimmunoassay (RIA) for the vitamin D-dependent 28,000 dalton calcium-binding protein. *Methods Enzymol.* 1983;102:291-6.

20. Graeff-Armas LA, Kaufmann M, Lyden E, and Jones G. Serum 24,25-dihydroxyvitamin D. *Clin Nutr.* 2018;37(3):1041-5.

21. Ong L, Saw S, Sahabdeen NB, Tey KT, Ho CS, and Sethi SK. Current 25-hydroxyvitamin D assays: do they pass the test? *Clin Chim Acta.* 2012;413(13-14):1127-34.

22. Hedman CJ, Wiebe DA, Dey S, Plath J, Kemnitz JW, and Ziegler TE. Development of a sensitive LC/MS/MS method for vitamin D metabolites: 1,25 Dihydroxyvitamin D2&3 measurement using a novel derivatization agent. *J Chromatogr B Analyt Technol Biomed Life Sci.* 2014;953-954:62-7.

23. Smith KW, Flinders B, Thompson PD, Cruickshank FL, Mackay CL, Heeren RMA, et al. Spatial Localization of Vitamin D Metabolites in Mouse Kidney by Mass Spectrometry Imaging. *ACS Omega.* 2020;5(22):13430-7.

24. Rowling MJ, Gliniak C, Welsh J, and Fleet JC. High dietary vitamin D prevents hypocalcemia and osteomalacia in CYP27B1 knockout mice. *J Nutr.* 2007;137(12):2608-15.

25. Elmore SA. Enhanced histopathology of the spleen. *Toxicol Pathol.* 2006;34(5):648-55.

26. Giavarina D. Understanding Bland Altman analysis. *Biochem Med (Zagreb).* 2015;25(2):141-51.

27. Hanel A, Veldhuizen C, and Carlberg C. Gene-Regulatory Potential of 25-Hydroxyvitamin D. *Front Nutr.* 2022;9:910601.

28. Wilhelm F, Mayer E, and Norman AW. Biological activity assessment of the 26,23-lactones of 1,25-dihydroxyvitamin D3 and 25-hydroxyvitamin D3 and their binding properties to chick intestinal receptor and plasma vitamin D binding protein. *Arch Biochem Biophys.* 1984;233(2):322-9.

29. Kutner A, Link RP, Schnoes HK, and DeLuca HF. Photoactivable analogs for labeling 25-hydroxyvitamin D3 serum binding protein and for 1,25-dihydroxyvitamin D3 intestinal receptor protein. *Bioorg Chem.* 1986;14:134-47.

30. Heine G, Niesner U, Chang HD, Steinmeyer A, Zugel U, Zuberbier T, et al. 1,25-dihydroxyvitamin D(3) promotes IL-10 production in human B cells. *Eur J Immunol.* 2008;38(8):2210-8.

31. Boonstra A, Barrat FJ, Crain C, Heath VL, Savelkoul HF, and O'Garra A. 1alpha,25-Dihydroxyvitamin d3 has a direct effect on naive CD4(+) T cells to enhance the development of Th2 cells. *J Immunol.* 2001;167(9):4974-80.

32. Rafique A, Rejnmark L, Heickendorff L, and Møller HJ. 25(OH)D3 and 1.25(OH)2D3 inhibits TNF-α expression in human monocyte derived macrophages. *PLoS One.* 2019;14(4):e0215383.

33. Nygaard RH, Nielsen MC, Antonsen KW, Højskov CS, Sørensen BS, and Møller HJ. Metabolism of 25-Hydroxy-Vitamin D in Human Macrophages Is Highly Dependent on Macrophage Polarization. *Int J Mol Sci.* 2022;23(18).

34. Liu N, Nguyen L, Chun RF, Lagishetty V, Ren S, Wu S, et al. Altered Endocrine and Autocrine Metabolism of Vitamin D in a Mouse Model of Gastrointestinal Inflammation. *Endocrinology.* 2008/10/01;149(10).

35. Cheng JB, Levine MA, Bell NH, Mangelsdorf DJ, and Russell DW. Genetic evidence that the human CYP2R1 enzyme is a key vitamin D 25-hydroxylase. *Proc Natl Acad Sci U S A.* 2004;101(20):7711-5.

36. Prosser DE, and Jones G. Enzymes involved in the activation and inactivation of vitamin D. *Trends Biochem Sci.* 2004;29(12):664-73.

37. Jones G, and Kaufmann M. Diagnostic Aspects of Vitamin D: Clinical Utility of Vitamin D Metabolite Profiling. *JBMR Plus.* 2021;5(12):e10581.

38. Kaufmann M, Schlingmann KP, Berezin L, Molin A, Sheftel J, Vig M, et al. Differential diagnosis of vitamin D-related hypercalcemia using serum vitamin D metabolite profiling. *J Bone Miner Res.* 2021;36(7):1340-50.

39. Kaufmann M, Martineau C, Arabian A, Traynor M, St-Arnaud R, and Jones G. Calcioic acid: In vivo detection and quantification of the terminal C24-oxidation product of 25-hydroxyvitamin D. *J Steroid Biochem Mol Biol.* 2019;188:23-8.

40. Ding N, Hah N, Yu RT, Sherman MH, Benner C, Leblanc M, et al. BRD4 is a novel therapeutic target for liver fibrosis. *Proc Natl Acad Sci U S A.* 2015;112(51):15713-8.

41. Ni L, Chen D, Zhao Y, Ye R, and Fang P. Unveiling the flames: macrophage pyroptosis and its crucial role in liver diseases. *Front Immunol.* 2024;15:1338125.

42. Steiniger BS. Human spleen microanatomy: why mice do not suffice. *Immunology.* 2015;145(3):334-46.

43. Adams JS, Chen H, Chun R, Ren S, Wu S, Gacad M, et al. Substrate and enzyme trafficking as a means of regulating 1,25-dihydroxyvitamin D synthesis and action: the human innate immune response. *J Bone Miner Res.* 2007;22 Suppl 2:V20-4.

44. Hewison M, Burke F, Evans KN, Lammas DA, Sansom DM, Liu P, et al. Extra-renal 25-hydroxyvitamin D3-1alpha-hydroxylase in human health and disease. *J Steroid Biochem Mol Biol.* 2007;103(3-5):316-21.

45. Pike JW, and Meyer MB. The unsettled science of nonrenal calcitriol production and its clinical relevance. *J Clin Invest.* 2020;130(9):4519-21.

46. Meyer MB, and Pike JW. Mechanistic homeostasis of vitamin D metabolism in the kidney through reciprocal modulation of Cyp27b1 and Cyp24a1 expression. *J Steroid Biochem Mol Biol.* 2020;196:105500.

47. Cantorna MT. Mechanisms underlying the effect of vitamin D on the immune system. *Proc Nutr Soc.* 2010;69(3):286-9.

48. Onal M, St John HC, Danielson AL, and Pike JW. Deletion of the Distal Tnfsf11 RL-D2 Enhancer That Contributes to PTH-Mediated RANKL Expression in Osteoblast Lineage Cells Results in a High Bone Mass Phenotype in Mice. *J Bone Miner Res.* 2016;31(2):416-29.

49. Tucker LH, Conde-González A, Cobice D, Hamm GR, Goodwin RJA, Campbell CJ, et al. MALDI Matrix Application Utilizing a Modified 3D Printer for Accessible High Resolution Mass Spectrometry Imaging. *Anal Chem.* 2018;90(15):8742-9.

50. Belov ME, Ellis SR, Dilillo M, Paine MRL, Danielson WF, Anderson GA, et al. Design and Performance of a Novel Interface for Combined Matrix-Assisted Laser Desorption Ionization at Elevated Pressure and Electrospray Ionization with Orbitrap Mass Spectrometry. *Anal Chem.* 2017;89(14):7493-501.

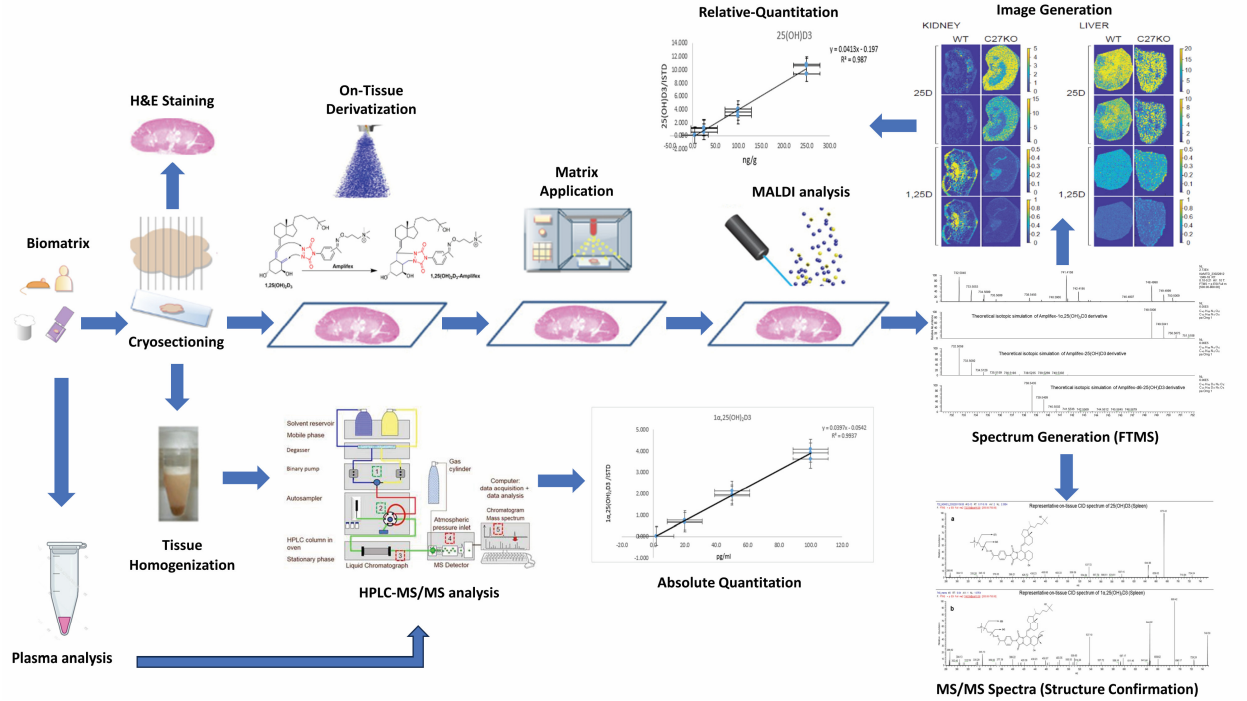

Figure 1: Mass spectrometry imaging workflow overview of tissue analysis. Isolated tissues are sectioned, and tissues samples are split for H&E staining, tissue homogenization (for absolute quantitation) and OTCD-MALDI-MSI for spatial distribution assessment and relative quantitation. Samples for OTCD-MALDI-MSI analysis undergo reagent application (Ampiflex®) with the inclusion of a stable isotope for relative quantitation and subsequent MALDI matrix application for MALDI-MSI analysis. Protonated ions for targeted metabolites are selected for image generation and relative quantitation with further ion isolation for structural confirmatory analysis (MS/MS) The plasma is taken for systemic metabolite contribution and analyzed by HPLC-MS/MS along with tissue homogenate for absolute quantitation of vitamin D metabolites.

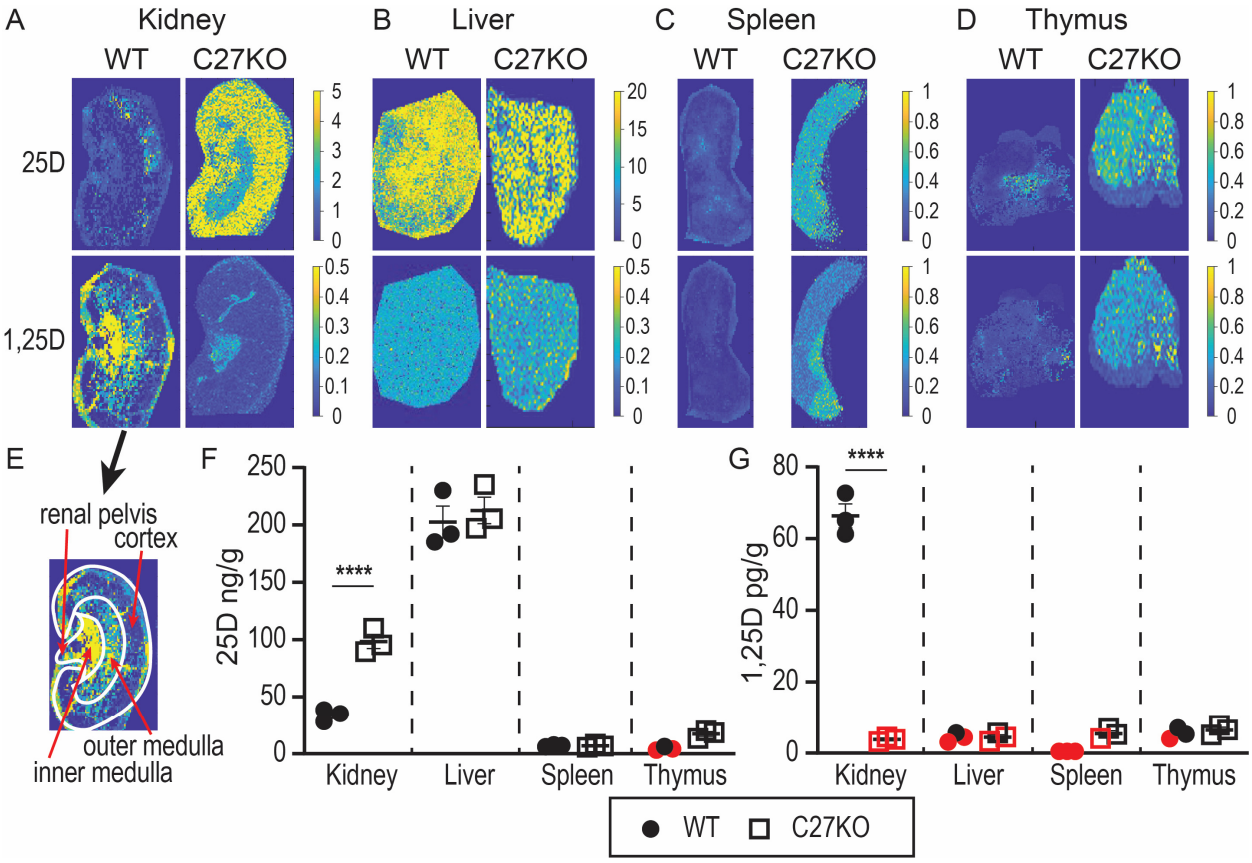

Figure 2: Tissue localization and relative quantitation of 25(OH)D_3 and 1,25$(OH)_2D_3$ in *Cyp27b1*-KO and WT mice. MALDI-MSI was performed on both *Cyp27b1*-KO and WT littermates in the kidney (A), liver (B), spleen (C), and thymus (D). Scale for each metabolite shown to the right of each tissue image (additional images in supplemental data). Intensity was normalized by stable isotope internal standard protonated mass. Signal intensity is depicted by parula color scale for semi-quantitative assessment on the scale shown. E, schematic of kidney anatomy overlaid with panel from 1,25D WT from (A). The relative quantitation of biological triplicates is shown for the 25(OH)D_3 (F, ng/g) and 1,25$(OH)_2D_3$ (G, pg/g) for each tissue (all values in Fig. S1). Data points that fall below the lower limits of quantitation (<LLOQ) but above the lower limits of detection (LLOD) are shown in red. n=3 for all tissues. Unpaired t-tests were performed: ****, $p<0.0001$ C27KO vs WT.

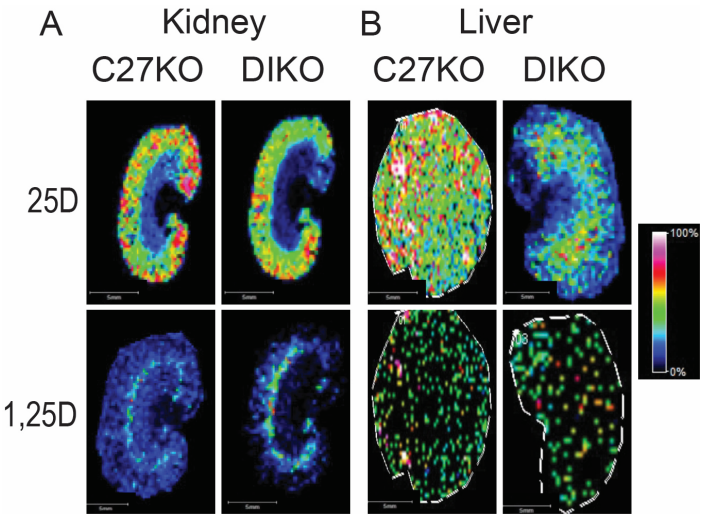

Figure 3: Qualitative Comparison of *Cyp27b1*-KO and M1/M21-DIKO mice by MALDI-MSI. MALDI-MSI was performed and the representative images from the kidney (A) and liver (B) for both the *Cyp27b1*-KO (C27KO) and M1/M21-DIKO (DIKO) mice and $25(OH)D_3$ (25D) and $1,25(OH)_2D_3$ (1,25D) were measured and displayed. The intensity scale used was based on total ion count (TIC) normalization using rainbow color scale.

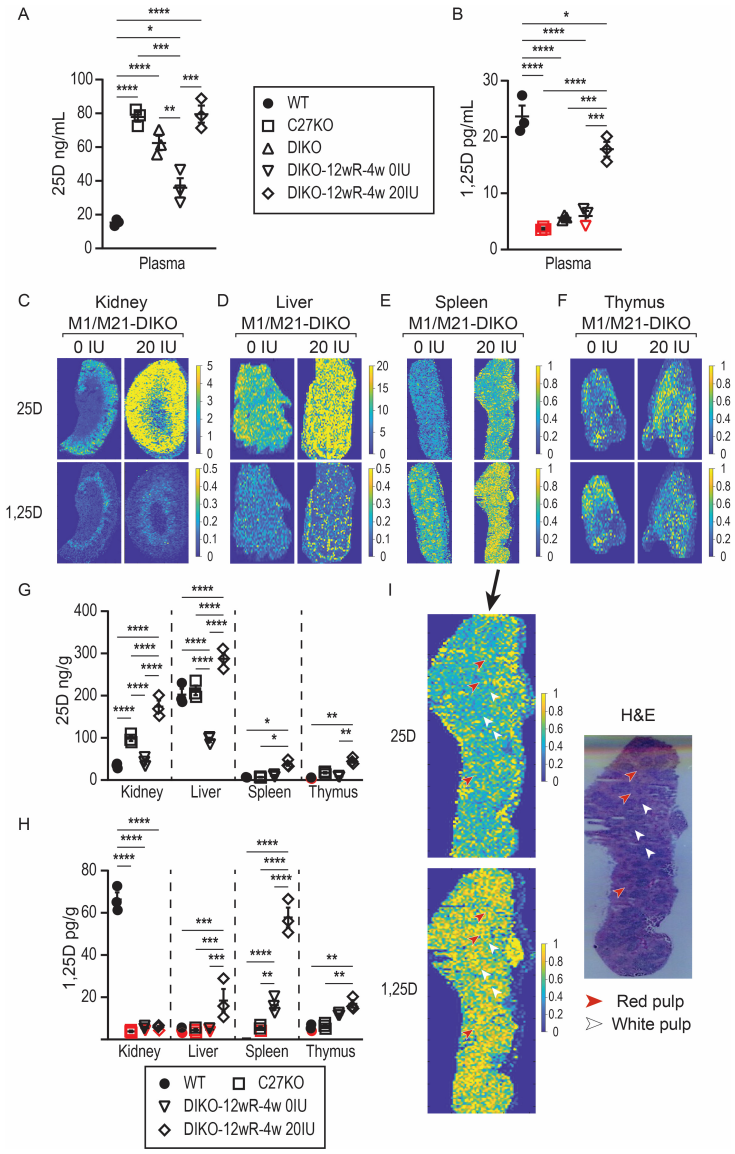

Figure 4: Detection of non-renal $1,25(OH)_2D_3$ production after vitamin D_3 supplementation. Plasma levels of $25(OH)D_3$ (A, 25D, ng/mL) and $1,25(OH)_2D_3$ (B, 1,25D, pg/mL) as detected by LC-MS/MS in the wildtype littermates (WT), *Cyp27b1*-KO (C27KO), M1/M21-DIKO (DIKO), M1/M21-DIKO 12 w rescue diet followed by 4 w of 0 IU vitamin D diet (12wR-4w 0 IU), and M1/M21-DIKO 12 w rescue diet followed by 4 w of 20 IU vitamin D diet (12wR-4w 20 IU). One-way ANOVA with multiple comparison Tukey post-test: *, $p<0.05$; **, $p<0.01$; ***, $p<0.001$; ****, $p<0.0001$, as indicated. MSI was performed and displayed for kidney (C), liver (D), spleen (E), and thymus (F) in the M1/M21-DIKO 12 w rescue diet followed by 4 w of 0 IU vitamin D diet (12wR-4w 0 IU) and M1/M21-DIKO 12 w rescue diet followed by 4 w of 20 IU vitamin D diet (12wR-4w 20 IU). Signal intensity is depicted by parula color scale for semi-quantitative assessment on the scale shown (additional images in supplemental data). The relative quantitation of biological triplicates is shown for the $25(OH)D_3$ (G, ng/g) and $1,25(OH)_2D_3$ (H, pg/g) for each tissue (all values in Fig. S1). Data points that fall below the lower limits of quantitation (<LLOQ) but above the LLOD are shown in red. n=3 for all tissues. One-way ANOVA (genotypes within tissues) with multiple comparison Tukey post-test: *, $p<0.05$; **, $p<0.01$; ***, $p<0.001$; ****, $p<0.0001$, as indicated. I, hematoxylin and eosin staining of thymus section with red and white pulp indicated. Overlaid data from spleen 25D and 1,25D panels from (E).

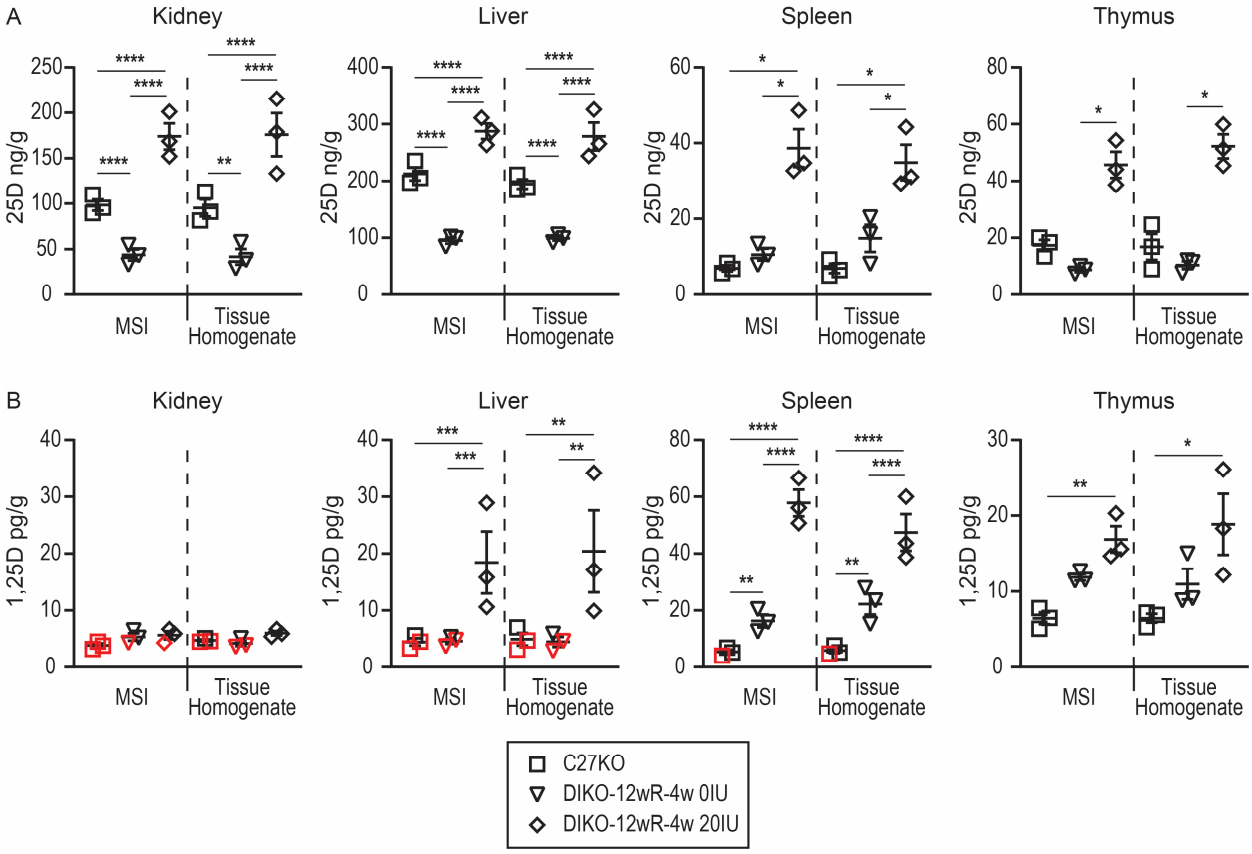

Figure 5: Confirmatory vitamin D metabolite levels in tissue homogenate. LC-MS/MS was performed on the remaining tissue not used for sectioning for 25(OH)D_3 (A, 25D, ng/g) and 1,25$(OH)_2D_3$ (B, 1,25D, pg/g) in the *Cyp27b1*-KO (C27KO), M1/M21-DIKO 12 w rescue diet followed by 4 w of 0 IU vitamin D diet (12wR-4w 0 IU), and M1/M21-DIKO 12 w rescue diet followed by 4 w of 20 IU vitamin D diet (12wR-4w 20 IU). Absolute quantitation of biological triplicates is shown for 25(OH)D_3 (A, ng/g) and 1,25$(OH)_2D_3$ (B, pg/g) for each tissue compared to the MSI values from Fig. 4 (all values in Fig. S1). Data points that fall below the lower limits of quantitation (<LLOQ) but above the LLOD are shown in red. n=3 for all tissues. One-way ANOVA (genotypes within tissues) with multiple comparison Tukey post-test: *, $p<0.05$; **, $p<0.01$; ***, $p<0.001$; ****, $p<0.0001$, as indicated. There were no differences between groups in MSI vs. Tissue Homogenate (by ANOVA and t-test).

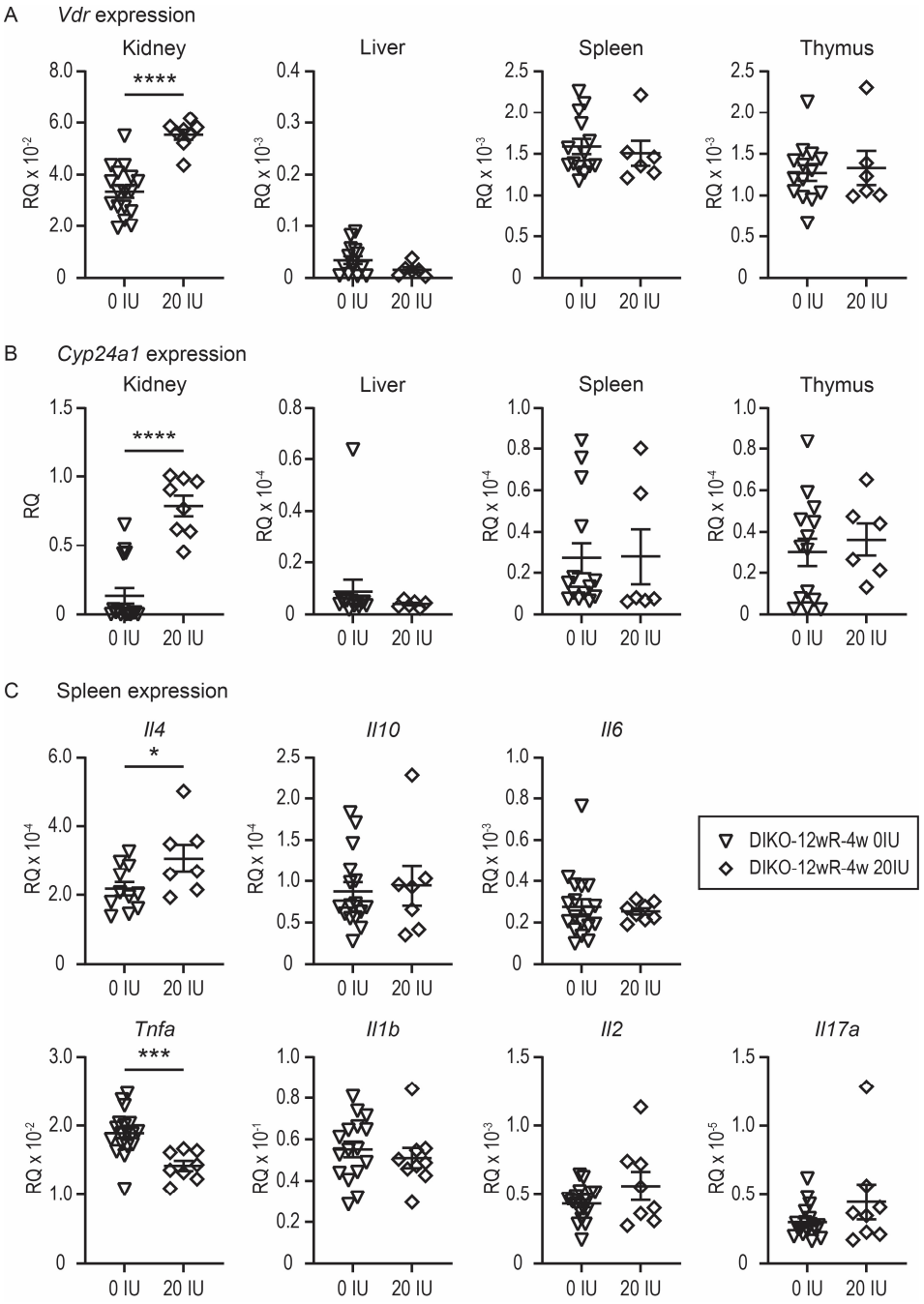

Figure 6: Gene expression changes in response to tissue elevations of $1,25(OH)_2D_3$. Gene expression was performed in the kidney, liver, spleen, and thymus for mice on the M1/M21-DIKO 12 w rescue diet followed by 4 w of 0 IU vitamin D diet (12wR-4w 0 IU, $n \geq 14$), and M1/M21-DIKO 12 w rescue diet followed by 4 w of 20 IU vitamin D diet (12wR-4w 20 IU, $n \geq 6$) for *Vdr* (A) and *Cyp24a1* (B). Cytokine gene expression was measured in the spleen for *Il4, Il10, Il6, Tnfa, Il1b, Il2*, and *Il17a* in the same diet conditions as A and B. Unpaired t-tests were performed: ****, $p<0.0001$; ***, $p<0.001$; *, $p<0.05$ - 20 IU vs 0 IU.